

Leveraging Activity Recognition to Enable Protective Behavior Detection in Continuous Data

Chongyang Wang

UCLIC, University College London, London, UK, chongyang.wang.17@ucl.ac.uk

Yuan Gao

Department of Information Technology, Uppsala University, Uppsala, Sweden, alex.yuan.gao@it.uu.se

Akhil Mathur

UCLIC, University College London, London, UK, akhil.mathur.17@ucl.ac.uk

Nicholas D. Lane

Department of Computer Science, University of Oxford, Oxford, UK, nicholas.lane@cs.ox.ac.uk

Nadia Bianchi-Berthouze

UCLIC, University College London, London, UK, nadia.berthouze@ucl.ac.uk

ABSTRACT

Protective behavior exhibited by people with chronic pain (CP) during physical activities is the key to understanding their physical and emotional states. Existing automatic protective behavior detection (PBD) methods depend on pre-segmentation of activity instances as they expect situations where activity types are predefined. However, during everyday management, people pass from one activity to another, and support should be delivered continuously and personalized to the activity type and presence of protective behavior. Hence, to facilitate ubiquitous CP management, it becomes critical to enable accurate PBD over continuous data. In this paper, we propose to integrate the automatic human activity recognition (HAR) with PBD via a novel hierarchical HAR-PBD architecture comprising GC-LSTM networks, and alleviate the data imbalances therein using a CFCC loss function. Through in-depth evaluation of the approach using a CP patients' dataset, we show that the leveraging of HAR, GC-LSTM networks and the CFCC loss function leads to clear increase in PBD performance against the state-of-the-art (macro F1 score of 0.81 VS. 0.66 and PR-AUC of 0.60 VS. 0.44). We conclude by discussing possible use cases of the HAR-PBD architecture in the context of CP management and other situations. We also discuss the current limitations and ways forward.

CCS CONCEPTS

•Applied computing~Life and medical sciences; • Computing methodologies~Supervised learning by classification

KEYWORDS

Chronic pain, protective behavior, activity recognition, deep learning, continuous data.

1 Introduction

Chronic pain is a prevalent condition suffered by ~30.7% of adults in US [77]. People with chronic musculoskeletal pain (a popular type of chronic pain) exhibit **protective behavior** (stiffness, hesitation, guarding, bracing and use of support) as they engage in physical activity [33]. Such behavior provides important information about the physical and emotional states of people and the ability to manage their condition [34, 35]. In clinical rehabilitation sessions, physiotherapists respond to the presence of such behavior by tailoring the level of encouragement and feedback they provide to patients as well as the type of management strategies and advices to apply [5]. This tailored support is critical to incrementally build patients' self-efficacy and maintain engagement with physical activity [36]. However, such service is

expensive and impractical given the prevalence of the CP population. In addition, according to clinicians [68], the behavior exhibited in the clinic falls short to fully portray physical and psychological capabilities of engagement in self-directed everyday physical activity. Unfortunately, self-management is hard and people often disengage with the daily tasks and job, with critical consequences on well-being and social life [34]. To be effective, observation and personalized support should extend outside the clinical context to help people self-manage their condition [37].

Ubiquitous sensing and computing technology offers new opportunities to provide such support to people with CP outside the clinic. It is reported by patients that a technology capable of protective behavior detection (PBD) could act as a ‘second pair of eyes’ to increase awareness of such behavior and aid with the application of pain management strategies learnt in the clinic [62]. In [79], patients and physiotherapists discuss how such technology could help patients e.g., to better control activity pacing and remember to breathe when protective behavior start to kick in. As physiotherapists do, the technology may also e.g., suggest adjusting the height of a chair if the patient was spotted to have difficulties sitting down or standing up. Findings from these studies also suggest that awareness of using protective behavior can help reduce protective behavior that has reached automaticity due to prolonged use of it (e.g., to remind them to bend the trunk as they stand up from a chair to facilitate the movement). In the addition to providing personalized feedback, such technology can be adopted to personalize and evaluate the effect of clinical interventions [65].

In order to build a ubiquitous technology that can help CP people in their everyday life, the first step is to enable continuous PBD as they engage in different functional activities. Until now, the focus has been to automatically detect protective behavior in the context of exercises where the activity being performed is known in advance. Indeed, interesting PBD results are only achieved within pre-segmented activity instances [40, 64]. Unfortunately, pre-segmentation is not feasible for everyday (functional) activities. In this paper, we aim to address such problems by tackling continuous PBD with continuous recognition of the activity (HAR) a person is engaged in. We propose a novel hierarchical HAR-PBD architecture to conduct continuous HAR plus PBD. The activity type being recognized is continuously leveraged to build **activity-informed** input for the simultaneous PBD.

To investigate the efficacy of our approach, we use the fully-annotated EmoPain dataset [32] which comprises the full-body movement data (18 IMUs) captured from healthy as well as CP participants engaged in sequences of movements reflecting everyday activities. We refer to these as Activity-of-Interests (AoIs) since they were chosen by physiotherapists as particularly demanding for CP people and tend to trigger protective behavior. It should be noted that while this dataset was not collected in the wild, participants were not instructed on how to perform each activity and the transition activities between AoIs created further noise typical of in-the-wild data collection. Indeed, during the transition periods, participants were allowed to rest according to their needs or enjoy any casual movement like turning around, walking and self-preparations. An illustration of a complete activity sequence of one CP participant along with the protective behavior annotation is shown in Figure 1.

The evaluation shows that the activity information noticeably improves the PBD performance on such continuous data, achieving macro F1 score of 0.73 and PR-AUC of 0.52 in comparison with the baseline method without such information (macro F1 score of 0.66 and PR-AUC of 0.44). Our contributions are:

1. A novel hierarchical HAR-PBD architecture, designed to leverage the activity recognition to enable the detection of protective behavior in continuous data sequences of AoIs and transition movements. For the first time, we empirically demonstrate the efficiency of using HAR to enable accurate continuous PBD.
2. Modeling the body-worn IMUs data as a graph sequence with a cascade combination of Graph Convolution (GC) and Long Short-Term Memory (LSTM) layers to address the high variability in body movement of both tasks. Whilst GC is used in computer-vision-based HAR systems, its efficacy in ubiquitous HAR and PBD has never been investigated.
3. Comprehensive experiments and analyses using data collected from CP patients, aimed to move a step closer to the deployment of our method in real-life scenarios. Various training strategies of our proposed hierarchical architecture are explored. A comparison on IMUs number is also conducted, which proves the possibility of using a smaller sensor set yet to achieve comparable PBD performances.

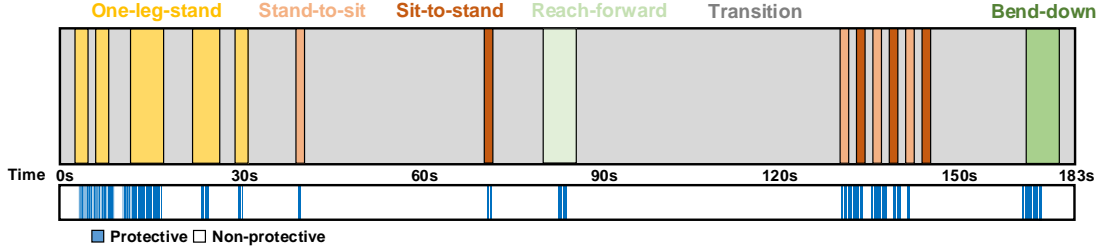


Figure 1: An example of continuous EmoPain data sequence from a CP participant showing different instances of AoIs and transition activity (in grey). Presence of protective behavior as labelled by clinicians (majority voting) is indicated in blue at the bottom of the sequence.

2 Related Work and Background

Our proposed hierarchical HAR-PBD architecture comprises two main modules: one for activity recognition and another for protective behavior detection. Here, we summarize the literature related to pain-, fear- and anxiety-induced movement behavior detection and human activity recognition.

2.1 Affective movement behavior detection

Pain, fear and anxiety are not expressed only through the face, but also by the way body movements are altered as any other affective or cognitive state does [2, 80]. The automatic detection of affective bodily expressions has become a growing area of research in the affective computing community [3, 74]. While in the past bodily expressions of emotion were studied in isolation, the focus is currently on real-life datasets. Due to the technical challenge, most studies still consider situations where people are static (e.g., during a consultation interview with a psychologist in the context of depression [6]) or the type of activity performed remains constant throughout (e.g., the detection of pain and anxiety in game-based physical rehabilitation [71, 78]). The bodily expression is also used to inform healthcare applications, e.g., for the detection of depression [6], oral hygiene behavior [7] and assessment for perinatal stroke screening in infants [8]. Typically, these scenarios only require the tracking of few body parts while a fine-grained analysis of full-body movement is not needed.

Automatic detection of continuous affective behavior across different daily activities is still rare. For example, [4] explored the detection of body expressions of reflective thinking in the context of diverse full-body mathematical games. While this study developed activity-independent models over continuous data sequences, their proposed LSTM-based architecture needs to be trained on pre-segmented affective events (e.g., when the child expresses the states of interest VS. other states). Recently, studies very relevant to ours have attempted to detect protective behavior across different activities. Using the EmoPain dataset [32], researchers have shown that the use of LSTM-based architectures facilitate activity-independent PBD with improved performances. Interesting results are seen in [40] and [64], where a stacked-LSTM network and body attention network (BANet) were proposed to conduct traversal and local processing of body movement data respectively. Despite the model is activity-independent and functions across different activity types, continuous detection was constrained only within pre-segmented AoIs. The relationship between the type of activity and protective behavior is not leveraged in the modeling. The attention mechanism used in BANet only focuses on identifying the most relevant body segments but does not directly leverage such relationship.

As such, how to enable continuous PBD along a sequence of activities remains an open challenge. The high variability of protective behavior across people exhibited within the same activity type [64] also calls for a better approach to extract useful information from the full-body configuration data.

2.2 Automatic human activity recognition

The modeling of body movement has gone through extensive development in the context of human activity recognition (HAR). The majority of HAR research focuses on classifying the type of activity a person is engaged in by using wearable sensor data [9-16] or skeleton data collected via visual motion-capture

(MoCap) systems [17, 18]. The preference of wearable sensors VS. visual systems lays upon the level of mobility imposed by the application.

HAR with vision- and sensor-based data has evolved a lot in the past several years, especially from the perspective of data processing. Initially, similar to the work in affective computing, data were processed in a traversal manner, where acceleration, orientation or joint positional coordinates were treated as temporal multi-dimensional sequences. As a result, efforts were dedicated to feature engineering [38, 39] and basic neural networks [9-11] e.g., LSTM networks [61], to address the temporal aspects of body movement data. Later on, various studies have started to exploit the spatial configuration of the sensor/joint. For instance, several data representations have been explored, which consider the relative relationships between sensors/joints [41-43] with network architectures designed to enable a local-processing of movement dynamics [12, 13, 44-46, 64]. The reported performance improvements achieved by these methods suggest that the body configuration is indeed important for activity recognition. More recently, the re-introduction of graph convolution network (GCN) [54, 55] has opened a new way for HAR. One reason for the successful use of GCN on visual MoCap data is that human body can be naturally presented as a non-directed graph. Such graph representation helps a model learn the biomechanical relationships between body segments without imposing knowledge about the specific activities of interest. Noticeable improvements are seen on several benchmark datasets (e.g., NUS RGB+ [19] and Kinetics [20]), achieved by recent studies using GCNs.

Whilst the concept of body configuration is very much leveraged in vision-based HAR systems, as it is enabled by the full-body capturing therein, it is not the case for ubiquitous sensor-based HAR or movement behavior detection literature. The sensor-based HAR literature has focused on using a small set of sensors to classify activity. One reason is that each study has looked into very specific activities [15] or benchmark datasets [21-23]. The rationale for using a small network of sensors is also to increase applicability and reduce cost in real-life deployment. However, as in the case of chronic-pain everyday rehabilitation, the critical information may not be in the movement of the main body segments involved in the activity, but in several different body parts recruited to protect the body [33-36]. For example, a study by Olugbade et al [37] shows the importance of head stiffness in detecting protective behavior during sit-to-stand-to-sit and reach-forward, despite the head movement is not needed to perform such activities. Psychology studies in chronic pain point to the importance to measure movement qualities and not just the amount of activity performed. This is critical to the evaluation of the psychological capability of a person to engage in physical activity, and to reduce pain not for the condition but for anxiety or repetitive maladaptive behavior [5]. As a result, the use of full-body movement data (as in the case of the EmoPain dataset) rather than a very small set of sensors, in PBD across activity, is based on three arguments: i) full-body movement data is needed to capture detailed movement behavior of local body parts and enable the detection of protective behavior across activities; ii) patients and clinicians see benefits and opportunities that such sensing technology offers and they are open to the use of it [65]; iii) full-body sensing is becoming more convenient as wearable sensors are being made smaller and integrated into clothes [76].

The advantage brought by the use of GCN in HAR, the need to model a large set of sensors and the importance of local information for PBD suggest the importance of exploring the use of GCN in the context of protective behavior. In addition, it is surprising the research of HAR and PBD (or in general emotional movement behavior detection) have evolved separately, as they are clearly representing activity and emotional bodily expression co-occur in everyday life, one altering the other. In this paper, we aim to use the proposed hierarchical architecture to answer the questions i.e., is HAR beneficial to PBD in continuous data and how these two modules could be connected? For each module of our proposed architecture, graph convolution is employed to model the movement data captured by multiple IMUs per timestep. Given the previous success of LSTM in capturing the temporal pattern of protective behavior [40, 64], LSTM layers are added to model the temporal dynamics.

3 The Hierarchical HAR-PBD Architecture and CFCC Loss

A novel hierarchical architecture combining PBD with HAR modeling is proposed to enable PBD over continuous data sequences of activities. An overview of this architecture is presented in Figure 2. Both the

HAR and PBD modules receive consecutive frames extracted with a sliding-window from the data sequence collected with 18 IMUs as the input. For HAR module the activity type label is used for training, whereas for PBD the protective behavior label (absence and presence) is used. In addition, the first module (HAR) aims to recognize the type of activity being performed and pass such information to the second module (PBD) that recognizes the presence or absence of protective behavior. For our main experiments, the HAR module is pre-trained with activity labels on the same folds of data during each round of LOSO validation used for PBD, and the model with the weight achieving highest activity recognition accuracy is saved. The frozen HAR module with such pre-trained weight loaded is used in the hierarchical architecture, where its activity classification output is concatenated with the same original raw input frame and passed to train and test the PBD module using labels of protective behavior. We use this frozen (optimal) HAR module to better understand the benefit of using the proposed hierarchical HAR-PBD architecture. Further analyses using non-frozen HAR module are reported at the end of the paper. To the best of our knowledge, this is the first implementation to leverage the output of HAR to enable another simultaneous task on the same data input.

Both modules in our proposed architecture use a similar network comprising graph convolution and LSTM layers. The graph convolution method is used to model the body configuration information collected from 18 IMUs. Following its success in recent vision-based HAR literature, we aim to explore the contribution of graph convolution in PBD given the large variety in protective behavior exhibited by people with CP when performing each AoI, as shown in a later section. Meanwhile, LSTM is used to learn the temporal dynamics across graphs corresponding to the body movement at different timesteps, a critical information for both HAR and PBD (e.g., hesitation slows down movements, and fear of pain or perceived pain lead to difference in timing of body parts engagement for the same activity).

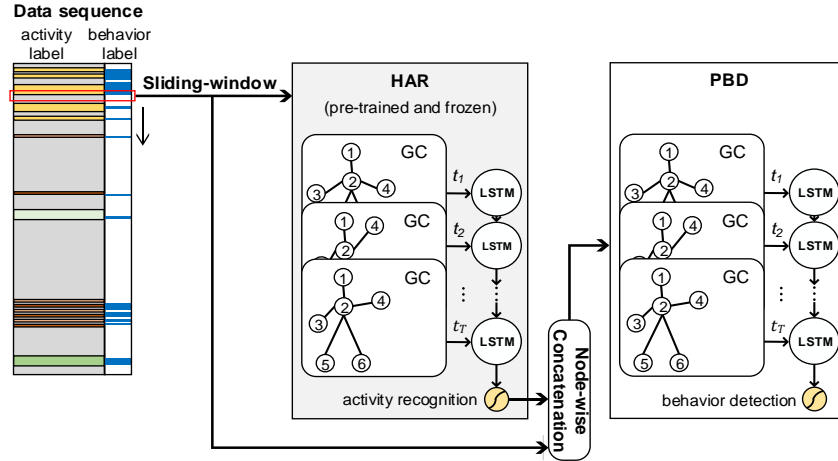


Figure 2: The proposed hierarchical HAR-PBD architecture, comprising the human activity recognition (HAR) module and protective behavior detection (PBD) module. The number of nodes (joints) used in this work is 22, instead of 6 as shown in the GC block above.

3.1 The HAR and PBD module with GC-LSTM

There are a variety of possible implementations of graph convolution for activity recognition. Some have altered the graph convolution itself to enable a spatial-temporal operation [17, 47-49]. Others integrate graph convolution with the gates of a LSTM unit [18, 24] to enable a recurrent computation across time. The performance of these approaches fluctuates on vision-based HAR benchmark datasets [19, 20]. For both the HAR and PBD module in our proposed architecture, a network integrating GC and LSTM is used, referred to as HAR/PBD GC-LSTM. Our main aim in this work is to understand its contribution to improve continuous PBD performances. At the same time, as GCN has been virtually unexplored within the context of sensor-based HAR, possibly due to the limited number of sensors normally used, this work also contribute to assess its use in a ubiquitous HAR context. There are three considerations for the design of GCN-LSTM:

- The limited volume of EmoPain dataset in comparison with popular vision-based HAR benchmarks [19, 20] that have been used to evaluate GCNs, which makes it more difficult to directly adopt existing more complex implementations.
- The need to verify if the graph representation is indeed capable of improving the detection of protective behavior, which requires to remove the interference e.g., the use of attention mechanism.
- The aim to connect the first module of HAR with the second module of PBD, which requires the graph network to tolerate the fusion of activity information and movement data at input level.

In this paper, we focus on a conceptually-simple implementation that builds cascade connection between the GC and LSTM as the basic component in our proposed architecture. Such implementation is able to show the advantage of using a graph representation to model data from multiple IMUs towards the joint objective of HAR and PBD, and further facilitates a hierarchical connection between the two modules.

3.2 Graph input

As provided in the EmoPain dataset [32], at each timestep, 3D coordinates of 22 body joints were calculated from the raw data of 18 IMUs stored in a Biovision Hierarchy (BVH) format. A wearable system named Animazoo ISG-190 comprising 18 IMUs was used for the data collection. As contained in the BVH file, the meta data includes the skeleton proportion of the participant (e.g., the length of arms) and position on the body at the time the sensor was attached. Using a Matlab MoCap toolbox [70], the approximate position of 22 body joints in 3D space were estimated based this initial information and the accelerometer data. It is important to note that such transformation has no prior knowledge of specific activities to be recognized. It only reflects the definite position of each joint in a 3D space. An illustration of such transformation from IMUs to the positional triplets of body joints forming the graph input is shown in Figure 3.

3.3 Graph notation

A body-like graph is built to arrange each of the 22 joints to be a node connected naturally in the graph to the other joints, as shown in Figure 3 (c). We denote the graph as $\mathcal{G} = (V, E)$, with a node set $V\{t, i\} = \{v_{ti} | t = 1, \dots, T; i = 1, \dots, N\}$ representing the N nodes of a graph at a timestep t within a graph sequence of length T , and an edge set E represents the edges connecting the nodes in this graph. In our case, $N = 22$ is in accord with the 22 body joints characterizing the EmoPain dataset, while only the intra-skeleton edge (representing the connection of body joints) is considered with $E\{i, j\} = \{(v_{ti}, v_{tj}) | (i, j) \in B\}$, where B is the set of naturally connected nodes (joints) of the human body graph. Since in this work independent LSTM layers are used to learn the temporal dynamics across graphs at different timesteps, the inter-skeleton edge (usually represent the temporal dynamics) connecting consecutive graphs is not leveraged. An adjacency matrix $\mathbf{A} \in \{0,1\}^{N \times N}$ is used to identify the edge E between nodes, where $A_{i,j} = 1$ for the connected i -th and j -th nodes and 0 for disconnected ones. \mathbf{A} stay the same for all the tasks in this work. In other words, the

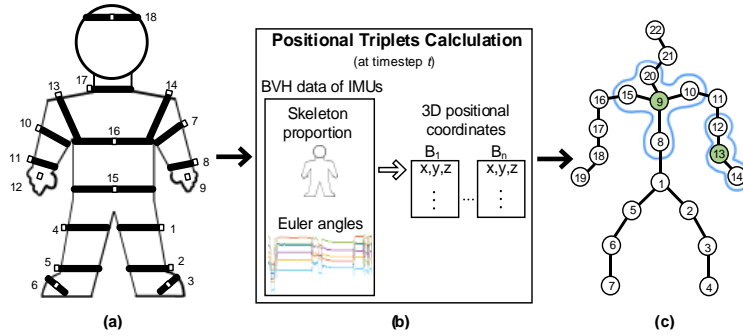


Figure 3: The illustration of (a) the placement of 18 IMUs, (b) the calculation of 22 sets of positional triplets, and (c) the built graph input at a single timestep, where each node represents a human body joint. The blue contour area is the neighbor set (receptive field) of the centered node in green.

basic configuration of a graph is independent of time and participants, while the relative relationship between different body parts in different activities are learnt during training. The identity matrix is \mathbf{I}_N , a diagonal matrix that represents the self-connection of each node in the graph. With the adjacency matrix \mathbf{A} and identity matrix \mathbf{I}_N , the human body configuration is represented by matrices that can be processed by neural networks. The feature of each node in a graph at timestep t is stored in feature matrix $\mathbf{X}_t^G \in \mathbb{R}^{N \times 3}$. For each node in the input graph, the raw feature is the coordinates of the respective body joint, denoted as $\mathbf{X}_t^G(v_{ti}) = [x_{ti}, y_{ti}, z_{ti}]$. The neighbor set of a node v_{ti} is denoted as $\mathcal{N}(v_{ti}) = \{v_{tj} | d(v_{ti}, v_{tj}) \leq D\}$, with distance function $d(v_{ti}, v_{tj})$ accounting for the number of edges in the shortest path traveling from v_{ti} to v_{tj} and threshold D defining the size of the neighbor set.

3.4 Graph convolution

Basically, a graph convolution comprises two parts, one defines the way to sample data from the input graph and the other concerns assigning learnable weight to the sampled data. It should be noted that a higher-level knowledge about the subset of body parts relevant to specific activities is not manually provided in the network. Therefore, only low-level rules of sampling and weighting are defined in the graph convolution, which allows the network to develop its own understanding about the body movement. In our case, the graph convolution needs to conduct sampling on the full-body graph comprising 22 nodes. We follow the basic derivation of GCN presented in [17], and the graph convolution used in this work is written as

$$f_{out}^{GC}(v_{ti}) = \sum_{v_{tj} \in \mathcal{N}(v_{ti})} \frac{1}{Z_{ti}(v_{tj})} f_{in}^{GC}(\mathbf{p}^{GC}(v_{ti}, v_{tj})) \cdot \mathbf{w}^{GC}(l_{ti}(v_{tj})), \quad (1)$$

where graph-adapted sampling function is $\mathbf{p}^{GC}(v_{ti}, v_{tj}) = v_{tj}$ with $d(v_{ti}, v_{tj}) \leq 1$, the graph-adapted weight function is $\mathbf{w}^{GC}(v_{ti}, v_{tj}) = \mathbf{w}'(l_{ti}(v_{tj}))$ with $l_{ti}(v_{tj}) = d(v_{ti}, v_{tj})$ and \mathbf{w}' to be the trainable weight matrix, f_{in}^{GC} is the input feature of the sampled node set at current layer while f_{out}^{GC} is the output feature of the respective centered node v_{ti} , and $Z_{ti}(v_{tj}) = \mathbf{card}(\{v_{tk} | l_{ti}(v_{tk}) = l_{ti}(v_{tj})\})$ is a normalization term representing the cardinality of the partitioned subsets in the neighbor set. As we can see, given the sampling and weight functions used, the 1-neighbor set $\mathcal{N}(v_{ti}) = \{v_{tj} | d(v_{ti}, v_{tj}) \leq 1\}$ is applied to be the receptive field of each node v_{ti} , as depicted by the blue contour in Figure 3 (c). Within the weight function, the partition function $l_{ti}: \mathcal{N}(v_{ti}) \rightarrow \{0, \dots, K-1\}$ can be used under different strategies, while in our work the distance-partitioning strategy [17] is adopted that divides the 1-neighbor set $\mathcal{N}(v_{ti})$ into two subsets, namely the centered node v_{ti} and the remaining neighbor nodes $v_{tj} | d(v_{ti}, v_{tj}) \leq 1$. As a result, we have $K = 2$ subsets thus $l_{ti}(v_{tj}) = d(v_{ti}, v_{tj})$. By using the distance-partitioning strategy, $Z_{ti}(v_{tj})$ equals to the number of all the neighboring nodes v_{tj} within the same neighbor set because they are within the same subset as well.

Using the adjacency matrix \mathbf{A} and identity matrix \mathbf{I}_N , we follow the practical forward-passing formula of a graph convolution layer presented in [63] to rewrite the equation 1 into a more straightforward form as

$$\mathbf{f}_{out}^{GC} = \widehat{\mathbf{A}}^{-\frac{1}{2}} \widehat{\mathbf{A}} \widehat{\mathbf{A}}^{-\frac{1}{2}} \mathbf{f}_{in}^{GC} \mathbf{W}, \quad (2)$$

where $\widehat{\mathbf{A}} = \mathbf{A} + \mathbf{I}_N$ represents the inter- and self-connection of each node, and $\widehat{\mathbf{A}}_{ii} = \sum_j \widehat{\mathbf{A}}_{ij}$ is a diagonal degree matrix of $\widehat{\mathbf{A}}$. Since $\widehat{\mathbf{A}}$ is a positive diagonal matrix, the entries of its reciprocal square root $\widehat{\mathbf{A}}^{-\frac{1}{2}}$ are the reciprocals of the positive square roots of the respective entries of $\widehat{\mathbf{A}}$. Each diagonal value in the degree matrix $\widehat{\mathbf{A}}$ counts the number of edges connecting the respective node in the graph described by $\widehat{\mathbf{A}}$. Such transformation from \mathbf{A} to $\widehat{\mathbf{A}}$ is in accord with our choice of distance-partitioning, where each neighbor set is divided into two subsets for weight assignment, namely the center node (\mathbf{I}) and the neighbor nodes (\mathbf{A}). \mathbf{f}_{in}^{GC} is the input feature matrix, and $\mathbf{f}_{in}^{GC} = \mathbf{X}_t^G$ at the first layer of input level. \mathbf{W} is the layer-wise weight matrix.

3.5 Cascade connection of graph convolution and LSTM

Here, we describe how the GCN and LSTM layers are connected, as used in both the HAR and PBD modules of our hierarchical architecture. For each module, the input to a single unit in the first LSTM layer is the

concatenation of the graph convolution output from all the nodes in the graph \mathcal{G} at timestep t , denoted by $\mathbf{f}_{out}^{GC}(\mathbf{X}_t^G) = [f_{out}^{GC}(v_{t1}), \dots, f_{out}^{GC}(v_{tN})]^T$. We want to justify whether GCN improves the PBD performance or not, so the GCN and LSTM should not be integrated completely. For the adopted forward-processing LSTM layer, the computation at each LSTM unit is repeated to process the information across graphs from the first timestep to the last. As each LSTM unit at a timestep t receives the output from a graph convolution, we call such connection a **cascade connection** between the graph convolution and LSTM. Such conceptually-simple design involving the graph convolution only as a way to learn representations enables us to empirically study its impact on PBD performances. In comparison, others conducted the graph convolution within the gates of a LSTM unit [18, 24] or used extra computational blocks for application-specified purpose (e.g., pooling and attention mechanism used in image captioning [28]) between the GC and LSTM layers.

3.6 Hierarchical connection of HAR and PBD modules

Up until this point, the GC-LSTM network used in each model of our proposed architecture has been defined. Here, we describe how to connect the HAR and PBD module. In each module, a fully-connected softmax layer is further added to the GC-LSTM network for the classification purpose. Let the probability toward each class of the current input frame to be $\mathbf{P} = [p_1, \dots, p_K]$ with K denoting the number of classes and \mathbf{Y} to be the one-hot prediction. K is 6, including the 5 AoIs and transition activity class for the HAR module, and is 2 for protective and non-protective behavior of the PBD module. In our proposed architecture, to provide activity-informed input from HAR to PBD, a node-wise concatenation is conducted where the one-hot activity label \mathbf{Y}^{HAR} is added to the input matrix $\mathbf{X}_t^G(v_{ti}) = [x_{ti}, y_{ti}, z_{ti}]$ of each node in the graph input for PBD per timestep (see Figure 2). Namely, for the PBD module, activity-informed input feature matrix at a node v_{ti} in a single graph is $\mathbf{X}_t^{G,PBD}(v_{ti}) = [\mathbf{X}_t^G(v_{ti}), \mathbf{Y}^{HAR}]^T$. Since the raw graph input fed to the PBD module is joined by the output of the HAR module, we call such a **hierarchical connection** between the two.

3.7 Addressing data imbalances with CFCC Loss

A problem with non-acted movement datasets is class imbalance (e.g., datasets for HAR [21-23]). In the case of the EmoPain dataset, protective behavior is sparsely spread within the AoIs of each data sequence, while it is generally absent during transition activities (see Figure 1). Specifically, on average the AoIs represent only 31.71% of a participant’s data sequence, with the rest being transition activities. Furthermore, on average, samples labelled as protective behavior represents only 21.09% of a patient’s data sequence, with the rest labelled as non-protective. Beyond the specifics of EmoPain dataset, we can expect such problems to increase in real-life everyday data where people tend to avoid the AoIs either due to fear of increased pain or injury or because of their psychological state [37]. Typical approaches used to address data imbalances include: i) data re-sampling for each class, where samples are either duplicated from the less-represented class or randomly sampled from the majority class [81]; ii) loss re-weighting, e.g., setting higher weights for the less-represented class and lower weights for the majority class [82]. Unfortunately, these methods require manual interferences with data samples that could also harm the training of a model [60].

In our work, we propose to use a loss function that alleviates data imbalance during training. Generally, for the types of supervised learning taking place in our HAR and PBD modules, the following **categorical** cross-entropy loss (CCE) [66] would be used

$$\mathcal{L}_{categorical}(\mathbf{P}, \mathbf{Y}) = -\mathbf{Y} \log(\mathbf{P}), \quad (3)$$

where $\mathbf{P} = [p_1, \dots, p_K]$ is the classified probability distribution of an input frame over the K classes, and \mathbf{Y} is the respective one-hot categorical ground truth label with $\mathbf{Y}(k) = 1$ only for the ground truth class k . During training, the loss computed for each frame is added up to be the total loss for the model to reduce. Such function tends to put more attention on decreasing the loss in the majority class and ignores the (mis)classification of the less-represented classes (e.g., the AoIs classes in the HAR task or the protective behavior class in the PBD task).

To address this problem, we took inspiration from the research on automatic object detection. In the object detection domain, a binary data imbalance is caused by the smaller area covered by the object-of-interest and the larger objectless background. Two main approaches proposed in this direction are the focal

loss [59] and the class-balanced term [60]. Based on binary cross-entropy loss function [66], focal loss [59] applies a sample-wise factor function adjusting the weight for a sample based on its classification difficulty (defined by the classified probability toward the ground truth class). The Focal Loss (FL) together with binary cross-entropy (CE) can be written as

$$\text{FL}(p, y) = (1 - p)^\gamma \mathcal{L}_{\text{binary}}(p, y) = -(1 - p)^\gamma (y \log(p) + (1 - y) \log(1 - p)), \quad (4)$$

where p is the classified probability toward the positive class of the current data sample, y is the binary ground truth indicator with 1 for the positive class and 0 for the negative class. As we can see, the factor $(1 - p)^\gamma$ with tunable hyperparameter $\gamma \geq 0$ is added to the original binary cross-entropy loss. The intuition is to reduce the loss computed from data samples that are well-classified, while the threshold for judging whether a data sample is well-classified or not needs to be adapted given different datasets and is controlled by γ . The increase of γ will reduce the threshold, then data samples with comparatively lower classification probability toward the ground truth are treated as the well-classified.

In [60], the authors further revised the vanilla cross-entropy loss by adding a class-wise weight to each class based on the so-called effective number of samples within it. For the class c , the effective number of samples is denoted as $E_{n_c} = \frac{1 - \beta^{n_c}}{1 - \beta}$, with a hyperparameter β controlling how fast the effective sample number E_{n_c} grows when the real samples number n_c increases. The class-balanced term then used in their study is the reciprocal of E_{n_c} written as

$$\frac{1}{E_{n_c}} = \frac{1 - \beta}{1 - \beta^{n_c}}. \quad (5)$$

Unlike the binary imbalance caused by the object area and its useless background, in the HAR module, class imbalances exist among the 6 categories of activity, while in PBD both protective and non-protective classes share the same importance. Therefore, to adapt the focal loss and class-balanced term to our scenario, we replace the CE with CCE to combine the Equation 3-5 as

$$\text{CFCC}(\mathbf{P}, \mathbf{Y}) = -\frac{1 - \beta}{1 - \beta^{n_k}} (1 - \mathbf{Y}\mathbf{P})^\gamma \mathbf{Y} \log(\mathbf{P}), \quad (6)$$

where n_k is the number of samples of ground truth class k for the current input data frame. This revised function, referred to as **Class-balanced Focal Categorical Cross-entropy (CFCC)** loss function, will be used in our study. To the best of our knowledge, this is the first time such a combination has been used for the computation of multi-class categorical cross-entropy loss in HAR and PBD. With CFCC loss, we aim to alleviate the data imbalance during training and also to understand its importance in comparison with the other components of our architecture. The code for all the methods mentioned in Section 3 will be released.

4 Dataset, Validation Methods and Metrics

In this section, we first provide more details about the EmoPain dataset, and then describe the validation methods and metrics used in the experiments.

4.1 The EmoPain dataset

The EmoPain dataset [32] used in this study contains movement data collected with 18 IMUs from 12 healthy participants and 18 CP participants. The placement of IMUs is illustrated in Figure 3(a). Four wireless surface EMG sensors were also used and placed on the high and lower back of a participant to capture the muscle activity. In this paper, we focus on the IMUs data and leave the exploration of muscle activity data for future works. As part of the EmoPain dataset, the annotation of protective behavior was provided by four domain-expert raters, including 2 physiotherapists and 2 clinical psychologists. Each expert rater independently inspected the on-site video of each CP participant that was collected in synchrony with the wearable sensor data, and marked the timesteps where each period of protective behavior started and ended. The healthy participants were assumed to show no protective behavior despite may have their own idiosyncrasies.

A sequence of five functional activities was designed by physiotherapists, comprising one-leg-stand, reach-forward, stand-to-sit, sit-to-stand and bend-down. These activities were selected to reflect the physical and psychological capabilities necessary for carrying out everyday functioning, e.g., a person may need to

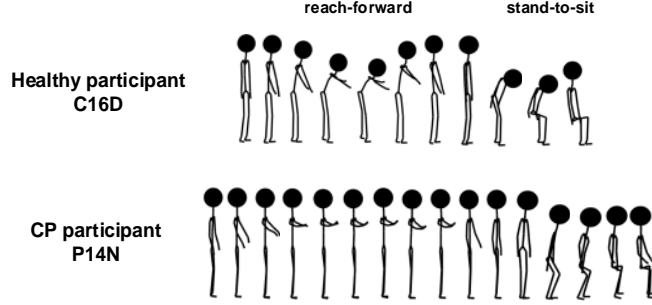


Figure 4: Examples of EmoPain movement data from healthy and CP participants. Different protective strategies can be seen in the activity performance by the CP participant: avoiding bending the trunk, twisting laterally the body to reach for the chair as support before sitting down.

reach forward to take an object placed on the far-end of a table, or **bend down** to load the wash machine. Avatar examples of a healthy and CP participant extracted from the dataset are provided in Figure 4. The figure illustrates two strategies used by this CP participant as forms of protective behavior: i) avoidance of bending the trunk during reach-forward; ii) hesitation, trunk twisting and shoulder side inclination for arm support during stand-to-sit.

Each participant went through at least one trial of the activity sequence, while 5 healthy and 11 CP participants executed both the normal and difficult trials. As a result, in total we have 46 activity sequences from 30 participants. During the normal trial, participants were free to perform these activities without any constraint. In the difficult trial, they were required to start the activity under the instruction of experimenters and carry an extra 2Kg weight in each hand during reach-forward and bend-down to simulate carrying everyday objects (e.g., shopping bags as typically suggested by physiotherapists). Such difficulty is added to collect the movement of a participant under external pressure or needs. However, no instructions of how a movement should be performed were provided, to ensure participants performed the activity in their own way as what they would do in real life. Between trails or even between activities, they were allowed to take break as needed and in the way they felt useful to relax or decrease muscle tension. The annotation of activity type was conducted manually by the EmoPain researchers, defining the starting and ending timesteps of each individual activity. In this study, we perform the following data preparations.

Raw Data as Input. Since the basic processing component of our proposed architecture operates on graphs that represent the configuration of the human body, the 3D coordinates of the 22 joints calculated from the 18 IMUs are directly used. This differs from previous studies [36, 37, 40, 64] on the same dataset, where low-level features as energies and angles between body segments were used. As described in Section 3.2, the approximate 3D joint coordinates were calculated from the BVH data returned by the wearable system (Animazoo ISG-190) using a Matlab MoCap toolbox [70]. The BVH data contains the skeleton proportion of each participant, sensor placements, and the accelerometer data sequences produced by the system at 60hz.

Continuous Data Segmentation with Sliding-window. Using a sliding window of 3s long and 50% overlapping ratio, each activity sequence of a complete trial of a participant is transformed into consecutive frames from the start of the first AoI to the end of the last AoI/transition activity. The window length and overlapping parameters are based on the evaluation studies reported in [40]. As the IMUs were operating at 60Hz, each frame contains 180 timesteps (samples). At timestep t , we have an input graph $\mathcal{G}_t = (V_t, E_t)$, represented by the input data matrix $\mathbf{X}_t^{\mathcal{G}}$, constant adjacency matrix $\mathbf{A} \in \{0,1\}^{22 \times 22}$ and its identity matrix \mathbf{I}_{22} , where $\mathbf{X}_t^{\mathcal{G}}(v_{ti}) = [x_{ti}, y_{ti}, z_{ti}]$, $v_{ti} \in V_t$. These matrices only represent the graph structure and raw coordinate data of each joint. The graph structure simulating the human body includes the set of nodes and their connections, i.e., it is the same for all participants across all activities. The activity class ground truth, i.e. one-leg-stand, reach-forward, sit-to-stand, stand-to-sit, bend-down and the transition, of a frame is defined by applying majority-voting to the 180 samples within it. The protective behavior ground truth of a

frame is also decided by majority-voting across the 4 domain-expert raters in accord with [40, 64], where a frame is labelled as protective behavior if at least 50% of the samples within it had been considered as protective behavior by at least two expert raters.

Data Augmentation. In order to address the limited size of the EmoPain dataset, we apply data augmentation techniques that have shown clear improvements in performance in previous works on the same dataset [40, 64], namely Jittering and Random Discarding. In jittering, normal Gaussian noise is globally applied with standard deviation of 0.05 and 0.1 separately to the original data. In random discarding, data samples at random timesteps and nodes are set to 0 with selection probabilities of 5% and 10%. The original number of frames produced with the sliding-window segmentation from all participants is ~ 6200 , while this number is increased to $\sim 31K$ after the augmentation.

4.2 Validation, metrics and implementations

For all the experiments, a Leave-One-Subject-Out cross validation (LOSO) is applied, which means that both the normal and difficult trails are left out for the subject if conducted. For HAR, we report the accuracy (Acc) and macro F1-score (Mac.F1) to account for the performance of all classes [72]. For PBD, aside from the Acc and Mac-F1, as a ‘binary’ task suffering from data imbalance, we additionally use the protective-class classification output acquired from all folds to plot Precision-Recall curves (PR curves) and report the Area under the Curve (PR-AUC) [73].

A search on number of layers, kernels and units for graph convolution and LSTM is conducted to identify the optimal hyperparameter set for the HAR/PBD module separately: i) for HAR, we use one graph convolution layer with 26 convolution kernels, three LSTM layers with 24 hidden units of each and one fully-connected softmax layer with 6 nodes for output; ii) for PBD, we use three graph convolution layers with 16 convolution kernels of each, three LSTM layers with 24 hidden units of each and one fully-connected softmax layer with 2 nodes for output. If not mentioned, the default loss function used for all the methods is the vanilla categorical cross-entropy described in Equation 3. In CFCC loss, the class-balanced term does not vary per sample, instead it is acquired for a class given the number of samples therein, so is computed and fixed before network training. To this end, we first conduct a hyperparameter search on $\gamma = \{0, 0.5, 1, 1.5, 2, 2.5\}$ and $\beta = \{0.9991, 0.9995, 0.9999\}$ for both tasks separately using the respective HAR or PBD module alone. We find $\gamma = 0.5, \beta = 0.9999$ to be the optimal for HAR and $\gamma = 2, \beta = 0.9999$ for PBD. Thereon, we compute the class-balanced term for each class of HAR and PBD. The Adam algorithm [67] is used as optimizer for all the models, while the learning rate is set to $5e^{-4}$ for the HAR module and $1e^{-3}$ for PBD module after another search on $lr = \{1e^{-5}, 5e^{-5}, 1e^{-4}, 5e^{-4}, 1e^{-3}, 5e^{-3}\}$. The OPTUNA framework [30] is used to conduct all the hyperparameter tuning. The number of epochs is set to 100.

In the first experiment, we report the baseline results of stacked-LSTM [40] and BANet [64], which represent the state-of-the-art on the EmoPain dataset for PBD, even though in their original studies only pre-segmented activity instances were used. We report the results for these two methods using the input of either i) 13 joint angles plus 13 energies as were used in the original studies, and ii) the coordinates of 22 joints calculated from 18 IMUs as were used in our proposed method. For stacked-LSTM, at each timestep we merely concatenate the coordinates of 22 joints to form the input matrix with a dimension of $22 \times 3 = 66$. Accordingly, the input structure of BANet is adapted for 22 pairs of coordinates as shown in Figure 5. The hyperparameters of the two models are also determined via a similar hyperparameter search as above.

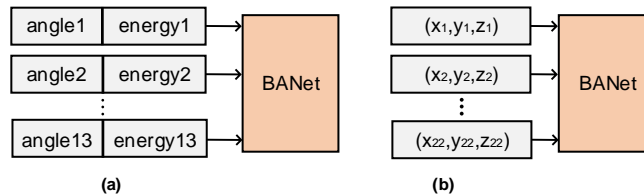


Figure 5: a) the original BANet input structure; b) the adapted BANet input structure for raw coordinates.

5 Results

The evaluation concerns several components of our proposed hierarchical HAR-PBD architecture, namely the contribution of graph convolution, CFCC loss and HAR to PBD performances. We then compare the HAR-PBD architecture in continuous data with its possible variants on pre-segmented data without the use of activity recognition. A visualization is also provided to highlight the effectiveness of our proposed method. We conclude by evaluating different training strategies of the HAR-PBD architecture, and its performance under different sizes of the IMUs network.

5.1 Contribution of GC to PBD

The first aim of our evaluation is to understand the contribution of graph representation in comparison with other approaches to the PBD performance. Hence, we conduct a set of experiments using the PBD module alone, without the use of the entire hierarchical architecture and the CFCC loss. The evaluation is conducted against the stacked-LSTM [40] and BANet [64] with either i) joint angles and energies; or ii) 22 pairs of coordinates as input. Differently from their original studies [40, 64] that relied on the pre-segmentation of activity instances, both methods are applied here over the full data sequences in a continuous manner.

Results are reported in Table 1 with PR curves plotted in Figure 6. As shown, the PBD GC-LSTM produces the best accuracy of 0.82, macro F1 score of 0.66 and PR-AUC of 0.44. The improvement in PR-AUC is more evident given its robustness to imbalanced data. The actual difference between these compared methods is the way the input data is processed, i.e., traversal concatenation (stacked-LSTM [40]), local processing (BANet [64]) and graph representation (PBD GC-LSTM). As such, the results suggest that the graph representation may indeed contribute to improving the detection of protective behavior. Still, the below-chance-level (<0.5) results of PR-AUC of all methods demonstrated the difficulty of continuous detection of protective behavior in the full data sequence across various activities. Indeed, even the accuracies for stacked-LSTM (angle + energy) and BANet (angle + energy) are lower than what reported in their original paper over pre-segmented activity instances, respectively accuracy of 0.8686 and 0.8688.

Table 1: PBD Results under different representation learning methods

Methods	Acc	Mac.F1	PR-AUC
Stacked-LSTM (angle+energy)	0.79	0.61	0.23
BANet (angle+energy)	0.78	0.56	0.24
Stacked-LSTM (coordinate)	0.80	0.64	0.32
BANet (coordinate)	0.79	0.63	0.27
PBD GC-LSTM	0.82	0.66	0.44

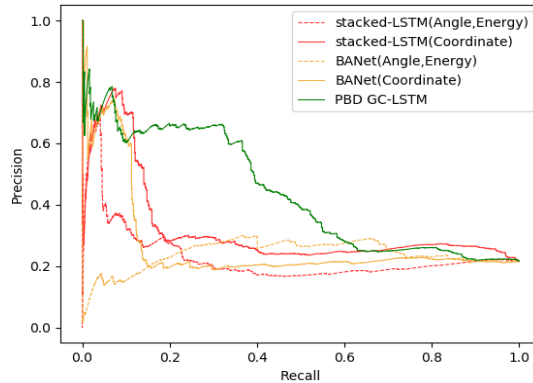


Figure 6: PR curves of different representation learning methods.

5.2 Ablation study

In this subsection, we first investigate the contribution of the loss function alone in dealing with the imbalanced dataset for each module of our proposed architecture. We then use our proposed hierarchical HAR-PBD architecture to understand the impact of activity-class information produced by the HAR module. In particular, we aim to understand if recognizing the activity background has more impact on improving PBD in continuous data sequences, in comparison with the issue of data imbalances during training.

Contribution of CFCC Loss Function to Continuous HAR. In our proposed hierarchical HAR-PBD architecture, the HAR GC-LSTM together with the CFCC loss function was firstly pre-trained on the same set of data using activity labels, then the weights achieving the best activity recognition performance across all participants were saved and frozen during the training of the entire architecture. For the training and testing of the hierarchical architecture, the HAR output was used as an auxiliary information to contextualize the PBD. Therefore, the accuracy of the HAR module is important. Here, we report the performance of the HAR GC-LSTM alone with and without the CFCC loss function. The results are reported in Table 2, with confusion matrices shown in Figure 7. The CFCC loss leads to a higher macro F1 score (0.81 VS. 0.79) in the continuous HAR. Judging from the confusion matrices, the CFCC loss reduces the classification bias towards the most represented class (the transition activity), which resulted in a lower accuracy through (0.89 VS. 0.88). These results show the effectiveness of the CFCC loss for balancing multi-class categorical loss computation, which was not directly evaluated in the original studies [59, 60].

Contribution of the CFCC Loss Function to Continuous PBD. Here we investigate the contribution of the CFCC loss function to continuous PBD using the PBD GC-LSTM. The input to PBD GC-LSTM is the raw coordinate data without activity-class information. As we can see from the result in Table 3, the use of the CFCC loss function leads to ~5% macro F1 score improvement in continuous PBD (macro F1 score of 0.71 VS. 0.66). Confusion matrices shown in Figure 8 (a) (b) suggest that the adapted CFCC loss function does indeed help penalize the bias towards more frequent class (non-protective class in this case) while improving the recognition of the less-represented one (protective class). However, the PR-AUC of 0.48 is still below chance level, suggesting that addressing data imbalance alone is not sufficient in continuous PBD.

Table 2: HAR results of the ablation study

Methods	Acc	Mac.F1
HAR GC-LSTM	0.89	0.79
HAR GC-LSTM with CFCC loss	0.88	0.81

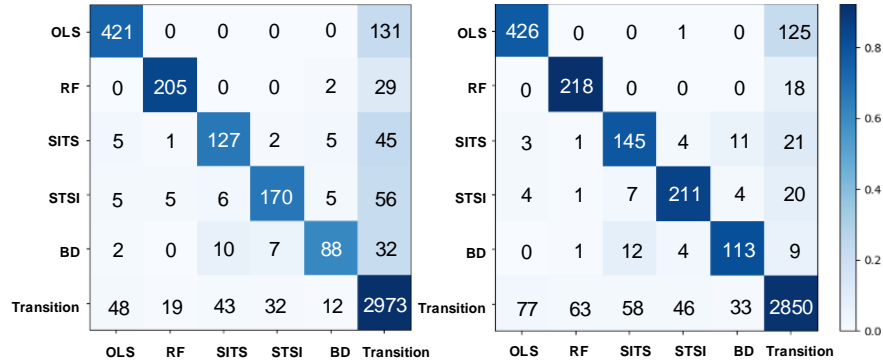


Figure 7: Confusion matrices for HAR GC-LSTM (left), HAR GC-LSTM with CFCC loss (right). OLS=one-leg-stand, RF=reach-forward, SITS=sit-to-stand, STSI=stand-to-sit and BD=bend-down.

Contribution of Hierarchical HAR-PBD Architecture to Continuous PBD. For the training and testing of our proposed hierarchical HAR-PBD architecture, the HAR GC-LSTM within it is frozen and loaded with the optimal weights from its pre-training with CFCC loss. This is to keep the HAR performance constant and aid the understanding of the impact of continuously inferred activity information on continuous PBD. The results are reported in Table 3, with confusion matrix shown in Figure 8 (c). It is interesting to see that our proposed hierarchical HAR-PBD architecture with vanilla categorical cross-entropy loss achieved an improvement of $\sim 2\%$ with respect to the PBD GC-LSTM alone using CFCC loss function (macro F1 score of 0.73 VS. 0.71), while the PR-AUC of 0.52 achieved is also above chance level. Such result implies that the contextual information of activity type contributes to continuous PBD with our proposed hierarchical HAR-PBD architecture being a practical way to leverage such information. Furthermore, by adding the CFCC loss function to the PBD module of the hierarchical HAR-PBD architecture, higher macro F1 score of 0.81 and PR-AUC of 0.60 are achieved (confusion matrix shown in Figure 8 (d)). The PR curves for the PBD ablation experiment are plotted in Figure 9 (left). These results show that the contextual information of activity types played a higher role in improving continuous PBD, while adding a mechanism (CFCC loss in our case) to address the dataset imbalance problem led to a further-clear improvement in performances. Such suggest that both the HAR and CFCC loss are necessary despite one being more informative than the other.

Comparison with Pre-segmented Approaches. Our proposed hierarchical architecture leverages the information of the activity background to assist continuous PBD. While this improves the performance, it remains unknown to which degree our approach is compared to the ones used on pre-segmented data without transition periods and that do not leverage activity type as contextual information. In this experiment, we compare our hierarchical architecture in continuous data with two-stage approaches on pre-segmented data of AoIs. Specifically, we compare our hierarchical HAR-PBD architecture (without CFCC loss for the PBD module) to a variant framework referred to as a *pre-segmented two-stage framework*. This modified framework adopts the stacked-LSTM/BANet/PBD GC-LSTM to process frames segmented from the data that is perfectly pre-segmented from the raw data sequence comprising the five AoIs only. For the hierarchical architecture, to enable such comparison, only performances acquired from the frames of five AoIs are

Table 3: PBD results of the ablation study

Methods	Acc	Mac.F1	PR-AUC
PBD GC-LSTM	0.82	0.66	0.44
PBD GC-LSTM with CFCC loss	0.83	0.71	0.48
Hierarchical HAR-PBD architecture	0.84	0.73	0.52
Hierarchical HAR-PBD architecture with CFCC loss	0.88	0.81	0.60

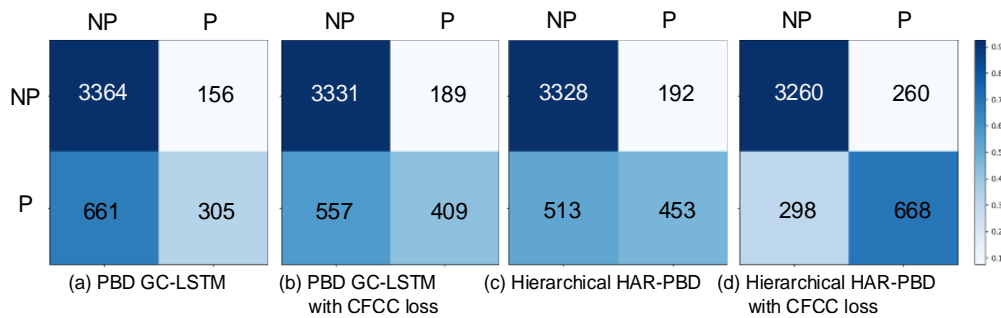


Figure 8: Confusion matrix of each method in the ablation study. ‘NP’ and ‘P’ is the non-protective and protective class respectively.

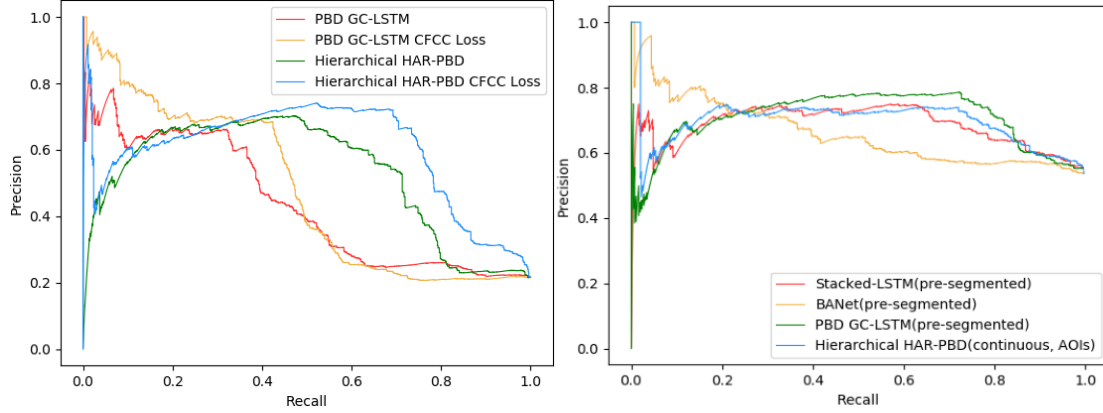


Figure 9: PR curves of (left) PBD methods in ablation study, (right) pre-segmented and continuous PBD methods.

included. Results are reported in Table 4 with PR curves plotted in Figure 9 (right). We find that, given a perfect segmentation of AoIs from the raw data, a notable gain in performance is achieved with macro F1 score of 0.74 and PR-AUC of 0.70, although such framework requires the complete data collection to be done beforehand and be pre-segmented. Still, our proposed hierarchical architecture applied to continuous sequence of data achieves a competitive PR-AUC of 0.69 (on AoIs), which is better than stacked-LSTM and BANet operated on the pre-segmented data. Given the results, it is also important to note that, as improvements in HAR (a very active area of work) are made, our framework will likely get improved since a sizable amount of inaccuracy in our framework is due to the fairly open problem of accurate HAR.

Table 4: PBD results of the pre-segmented and continuous methods

Methods	Acc	Mac.F1	PR-AUC
Stacked-LSTM (pre-segmented)	0.67	0.67	0.68
BANet (pre-segmented)	0.57	0.53	0.66
PBD GC-LSTM (pre-segmented)	0.74	0.74	0.70
Hierarchical HAR-PBD architecture (continuous, AoIs)	0.72	0.72	0.69

5.3 Performance analysis via visualization

To understand the temporal behavior of the two modules in the hierarchical HAR-PBD architecture, a visualized example of the model performances on the data of one CP participant is shown in Figure 10. The upper two diagrams are the ground truth and recognition result of the HAR module respectively. As shown, on this long data sequence, our HAR GC-LSTM using the CFCC loss achieves good performances without any pre-localization and -segmentation of the AOIs. The lower five diagrams are the ground truth and results of the PBD module achieved by the four different methods respectively.

In the HAR results (upper part of figure 10), the errors are found to be: i) misclassification of one-leg-stand as transition activity (red rectangle in the left); ii) misclassification of transition activities as reach-forward and bend-down (red rectangles in the middle); iii) misclassification of bend-down as stand-to-sit (red rectangle in the right). We notice that most misclassified activities were possibly due to their similarity in execution given the use of protective behavior by this CP participant. For instance, the analysis of the on-site video showed that the participant was unable to bend the trunk down and instead simply stretched both arms toward the ground, which is similar to the activity of reach-forward or transitions like standing still for rest.

We now compare the four PBD approaches (see M1-M4 in the lower part of Figure 10). Without the activity-class information and CFCC loss, the baseline PBD GC-LSTM (M1) misclassified most frames as the majority class of non-protective behavior. The use of CFCC loss (M2) and the activity-class information (M3) respectively enabled the model to detect more protective frames. For this CP participant, M3 is shown to be more effective than M2 in terms of detection at frame level of stand-to-sit, sit-to-stand and bend-down. The hierarchical HAR-PBD architecture with CFCC (M4) leads to the best result, especially for the detection at frame level of one-leg-stand. In the PBD result of the hierarchical architecture without CFCC loss (M3), the misclassified area marked by a red rectangle on the right side of the figure seems to be affected by the misclassification of a bend-down as stand-to-sit by the HAR module. Such error is corrected by using the CFCC loss function (M4). However, for the same approach (M4), the error marked by a red rectangle on the left side is likely to have been affected by the misclassification of one-leg-stand as transition activity by the HAR module. These results suggest that i) the misclassification in the HAR module has a negative impact on the PBD module; ii) in such case it is not sufficient to just use activity information (M3) but solving the data imbalance problem (M4) is also helpful. In other words, this supports our concept of approaching continuous PBD by addressing the two technical issues together, namely the contextual information of activity type and the imbalanced presence of protective behavior. As the recognition of activity type (HAR module) is challenged by the variety of protective behavior people use in performing an activity, it also becomes interesting to explore if the training of the PBD module may help improve the HAR performance when both are trained together. We discuss this in the next subsection.

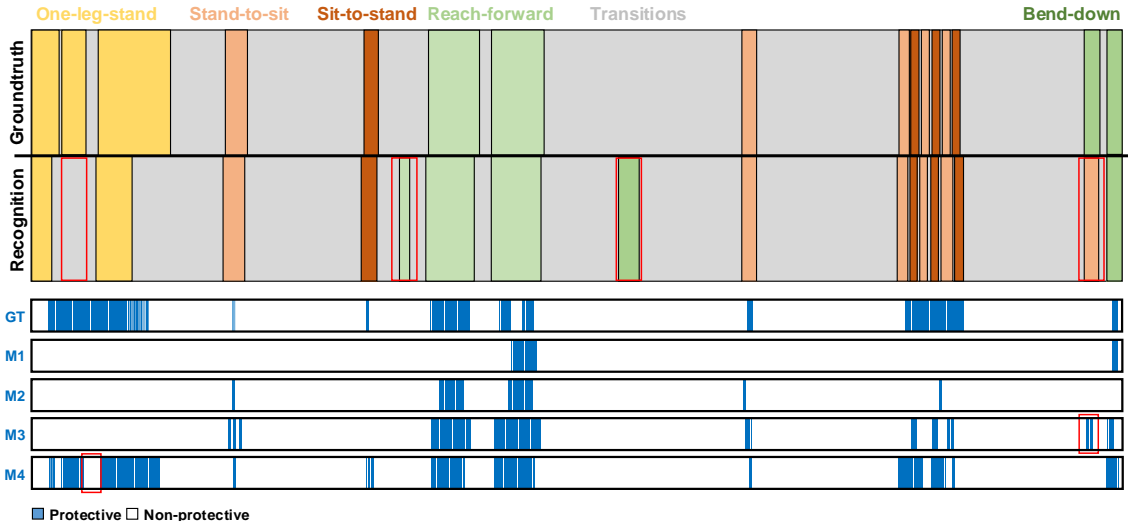


Figure 10: An example of the ground truth and results of HAR and PBD modules for the data of a CP participant. The upper diagram is showing the ground truth of activity class and the recognition result by HAR GC-LSTM with CFCC loss. At the lower diagram, the first row is presenting the ground truth of PBD. ‘M1’ to ‘M4’ are respectively the detection results for i) PBD GC-LSTM; ii) PBD GC-LSTM with CFCC loss; iii) hierarchical HAR-PBD architecture and iv) hierarchical HAR-PBD architecture with CFCC loss.

5.4 Training the hierarchical HAR-PBD architecture

In the previous subsections, the HAR module used in hierarchical HAR-PBD architecture was pre-trained with the same data using activity labels and frozen to adopt the model of optimal activity recognition performance. The aim was to understand the contribution of HAR to PBD across the different configurations. Here, we further explore the relationship between HAR and PBD modules by exploring joint-training strategies of the hierarchical architecture. In joint-training of the architecture, the HAR module would not be frozen but the activity labels would still be used to update it as the PBD module is trained. Meanwhile, the protective behavior labels of the same data input together with the output of HAR module are used for training

the PBD module. Namely, we compare the following four strategies while also explore the role of CFCC loss to HAR and PBD:

- i) **Joint HAR(CFCC)-PBD** and **Joint HAR-PBD(CFCC)**, where the HAR and PBD modules are initialized and trained together using activity and protective behavior labels respectively, with CFCC loss only added to either HAR or PBD module respectively;
- ii) **Joint HAR-PBD with CFCC**, where the CFCC loss is added to both modules in the joint training;
- iii) **Pre-trained Joint HAR(CFCC)-PBD** and **Pre-trained Joint HAR-PBD(CFCC)**, similar to (i) where the only difference is that the HAR module is first trained alone with activity labels to achieve the best activity recognition performance but then its training continues with the training of the PBD module;
- iv) **Pre-trained Joint HAR-PBD with CFCC**, where, after pre-training the HAR module to achieve the best HAR performance, CFCC loss is also added to the PBD module in the joint training.

For all these joint training strategies, the loss weights are set to $\{1.0, 1.0\}$ for both HAR and PBD modules. If the CFCC loss is not mentioned, the loss used for the respective module is the vanilla categorical cross-entropy loss. We also compare them with our proposed method used in previous sub-sections, here referred to as **Pre-trained HAR(Frozen)-PBD(CFCC)**, where the HAR module is first trained alone with activity labels and CFCC loss to achieve the best activity recognition performance per LOSO fold, then it is **frozen** with weights loaded and used in the hierarchical architecture for the training and testing of the PBD module. Results are reported in Table 5, with the PR curves for PBD results plotted in Figure 11 (left).

Without pre-training the HAR module, the best HAR (macro F1 score of 0.56) and PBD (macro F1 score of 0.74 and PR-AUC of 0.55) performances are achieved by the *joint HAR-PBD(CFCC)*. However, by adding CFCC loss to the HAR module alone (*joint HAR(CFCC)-PBD*), the performances are reduced notably for the HAR and slightly for PBD. One explanation could be that, the error passed back from the PBD module harmed the HAR performance, especially when such error of PBD was not well handled e.g., without using the CFCC loss function. On the other hand, by adding the CFCC loss to both modules (*joint HAR-PBD with CFCC*), the HAR performance achieved (macro F1 score of 0.54) is comparable to *joint HAR-PBD(CFCC)* but the PBD performance is much lower (macro F1 score of 0.71 and PR-AUC of 0.45). Given the current hierarchical architecture, such results suggest that alleviating the data imbalance in PBD has a stronger impact on the overall performance in joint training, while addressing it in HAR penalizes the PBD performance.

Rather than to start joint training from scratch, we further look into the uses of pre-training of the HAR module to reach an initial optimal activity recognition performance (macro F1 score of 0.81) before joint-training. A similar outcome as above is observed where the best performance is achieved by adding the CFCC

Table 5: Results for different training strategies of the HAR-PBD architecture

Training strategies	HAR		PBD		
	Acc	Mac.F1	Acc	Mac.F1	PR-AUC
Joint HAR(CFCC)-PBD	0.62	0.42	0.85	0.70	0.54
Joint HAR-PBD(CFCC)	0.76	0.56	0.84	0.74	0.55
Joint HAR-PBD with CFCC	0.66	0.54	0.81	0.71	0.45
Pre-trained Joint HAR(CFCC)-PBD	0.68	0.55	0.85	0.74	0.58
Pre-trained Joint HAR-PBD(CFCC)	0.84	0.73	0.87	0.79	0.58
Pre-trained Joint HAR-PBD with CFCC	0.72	0.64	0.85	0.76	0.55
Pre-trained HAR(Frozen)-PBD(CFCC)	0.88	0.81	0.88	0.81	0.60

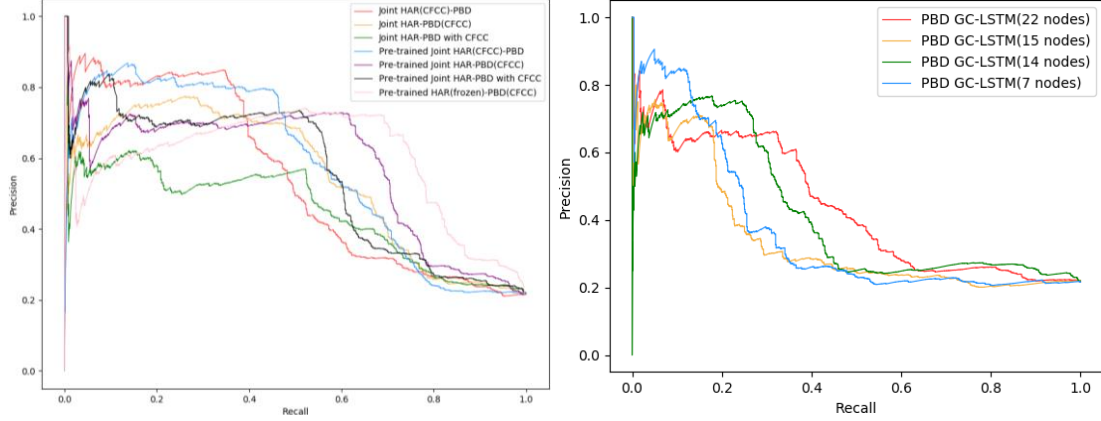


Figure 11: PR curves of (left) proposed hierarchical architecture under different training strategies, (right) PBD module with input of different number of nodes (joints).

loss to the PBD alone. Once again this proved the higher impact of alleviating the data imbalance of PBD, as the error passed back from the PBD module could harm the training of HAR module.

In general, the results show that a pre-training of the HAR module improved the final performances of both HAR and PBD modules in comparison to the ones without it.

The performance achieved by the various joint-training strategies of the hierarchical architecture are still lower than the one by freezing the HAR module as used in previous sub-sections, for both HAR (macro F1 score of 0.81) and PBD (macro F1 score of 0.81 and PR-AUC of 0.60). These results highlight the importance of HAR performance to PBD and suggest that the error propagated from the PBD to HAR module during joint-training was not informative to guide how the HAR module should be refined. In other words, given the current hierarchical architecture, the correctness of PBD during training does not necessarily inform the HAR module about the current activity input, which yet could be altered by the presence/absence of protective behavior. As a result, it is open for an exploration of better joint training strategy considering how the detection of protective behavior could improve the activity recognition. We leave this for future work.

5.5 Impact of the IMUs' number

In this final experiment, we evaluate the impact of reducing the number of IMUs to continuous PBD. Until this point, we have assumed all 18 IMUs to be available to enable the input of a full-body graph. In this experiment, we quantify the fluctuation in performance when fewer IMUs are available.

We simulate the limited availability of IMUs by removing specific nodes (containing the data of respective joints) from the full-body graph input of 22 nodes. First, a **reduced sensor set** is created to simulate the reduction of IMUs attached to the legs and arms by removing the nodes number 3, 6, 10, 12, 15, 17 and 21, resulting in a graph with 15 nodes. Second, a **smallest sensor set** is created by further removing the nodes number 4, 8, 11, 13, 16, 18 and 20, resulting in a graph with 7 nodes. To consider the case beyond removing nodes symmetrically from both sides of the full-body graph, a **one-sided sensor set** of 14 nodes is created as also mentioned in the study [36], where nodes number 2-4 and 10-14 on the left limbs of the body are removed. This is to reduce the sensor set size by removing possible redundant nodes/joints with respect to protective behavior. The graph structures of these sensor sets still simulate human body connections, as shown in Figure 12. The PBD module alone is used here without activity information and CFCC loss on the graph input extracted from each sensor set. For a fair comparison, we conducted another grid-search to determine the optimal hyperparameters under each condition, as detailed in Section 4.2. The results are summarized in Table 6, with PR curves plotted in Figure 11 (right). For the **reduced sensor set**, we observe a macro F1 score of 0.57 with PR-AUC of 0.34. Whereas, when using the **smallest sensor set**, the macro F1 score is reduced to 0.55 but with a higher PR-AUC of 0.37. In comparison with the default sensor set forming the graph input of 22 nodes (macro F1 score of 0.66 and PR-AUC of 0.44), the PBD performance under these sensor sets simulating fewer IMUs is clearly reduced. This supports one of the arguments we made about the

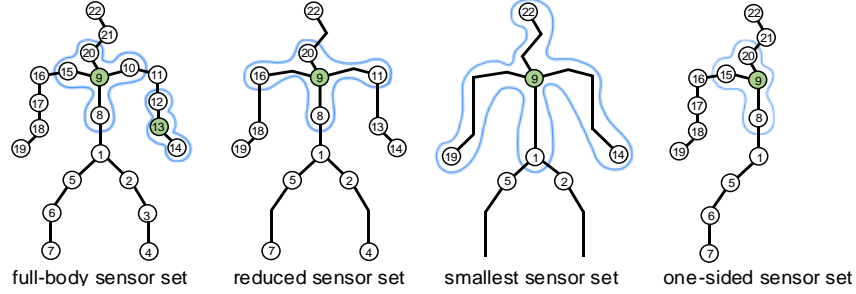


Figure 12: Graph structures of different sensor sets. The blue contours are the neighbor set of the centered node colored with green.

use of 18 IMUs (22 nodes), that the full skeleton data is needed to capture detailed movement behavior of local body parts in the case of PBD. On the other hand, a competitive result is achieved by the *one-sided sensor set* of 14 nodes (macro F1 score of 0.62 and PR-AUC of 0.42). Therefore, this provides an empirical verification that the PBD module (i.e., the GC-LSTM network) could function even with fewer IMUs, based on the observation that protective movement strategies are often visible on both sides of the body even if via different patterns e.g., a twisting of the trunk to reach for a chair may lead to a narrower angle between the arm and the trunk on one side but a compensatory larger angle between the other arm and the trunk. In the future, efforts can be made on i) designing better graph structure under a limited sensor set since in this work we merely employed the human-body joint connections; ii) leveraging the configurational characteristic of body movement, given the competitive performance achieved by the one-sided sensor set.

Table 6: Results of PBD module under different number of nodes (joints)

Number of Nodes (joints)	Graph structure name	Acc	Mac.F1	PR-AUC
22	Full body	0.82	0.66	0.44
15	Reduced sensor set	0.80	0.57	0.34
7	Smallest sensor set	0.81	0.55	0.37
14	One-sided sensor set	0.82	0.62	0.42

6 Discussion

Our long-term aim is to establish a ubiquitous system to support the self-directed management of people with CP in their everyday life. As the first step, we focused on the technical challenges of PBD in continuous data. We proposed a hierarchical HAR-PBD architecture to tackle the complex-varying activity background of protective behavior and a use of CFCC loss to alleviate the data imbalance of the real-patient dataset. We discuss here our open challenges, current limitations and possible use cases of the HAR-PBD architecture.

6.1 Technical challenges and current limitations

Our study explored the feasibility to continuously detect protective behavior across activities including transitions therein. Previous works on real-life continuous data in HAR and PBD have applied segmentation and localization of activities as an important first stage to get rid of unwanted data segments, using methods based on Hidden Markov Models (HMMs) [25], temporal characteristic of the movement [26] and pattern similarity [15, 27]. Instead, we operated on the continuous data sequence in a one-stage manner. This was achieved by leveraging continuous HAR together with the GC-LSTM network that improves the learning of bodily configurations and their temporal dynamics for both human activities and protective behavior. Further improvement in performances are obtained through the use of the adapted CFCC loss function. Our proposed hierarchical HAR-PBD architecture achieved the best macro F1 score of 0.81 and PR-AUC of 0.60 for PBD

in continuous data under LOSO validation. A good performance was also obtained for HAR with accuracy of 0.88 and macro F1 score of 0.81. Our in-depth studies show that the improvements in performances are mainly due to the leveraging of activity recognition. Overall, these results show feasibility of building a system that enable continuous tracking of protective behavior in everyday life where the activity performed is not known in advance. The main limitations of this work along with some possible solutions for the next-step are summarized as follows:

Limitations of Current Architecture Design. The best PBD performance so far achieved a macro F1 score of 0.81 and PR-AUC of 0.60, however, clearly a ubiquitous system would benefit from further improvements beyond these levels. Although such results are much higher than the baseline (macro F1 score of 0.66 and PR-AUC of 0.44), attention can be paid to several components of the architecture. For instance, in Section 5.4, we evaluated joint-training strategies of the hierarchical architecture. Interestingly, during joint-training of HAR and PBD modules, the CFCC loss function provides stronger contribution when used in the PBD module only. This could be because, by giving more importance to the loss related to the protective behavior class in PBD, the errors that propagated down to the HAR module possibly bring support to the recognition of AoIs classes, since these are the main source of protective behavior. Still, the best performance was achieved by pre-training and freezing the HAR module with CFCC loss instead of joint-training. As a future work, it would be hence interesting to explore how the recognition of PBD can be leveraged to support HAR recognition since the way an activity is performed can be altered by the expression of protective behavior.

Dependence on Manual Annotation. Our proposed architecture relies on manual annotations, particularly domain-expert ratings of protective behavior. For the expert annotation of protective behavior, our current practice of labelling frames by majority voting can be troublesome when disagreement exists. Toward this issue, we may consider methods like [69] to acquire a better consensus across experts.

6.2 Possible use cases

While the goal of this study was not to build a ubiquitous support system for pain management, our architecture is a critical component of such system as performances of continuous PBD are critical for effective support. It should also be noted that the contextualization provided by the HAR module not only leads to improved PBD performance but provides information to better assess CP people’s difficulties and customize timely support for self-management. We discuss here the three main use cases and further developments that can take advantage of our proposed HAR-PBD architecture to develop new types of support and interventions in chronic pain management and beyond.

In-The-Wild-Informed Clinical Rehabilitation. As pointed out in the introduction, clinicians consider movement observed in the clinic not very representative of patients’ physical and psychological capabilities to engage in their everyday tasks [68]. This is because patients may feel safer in the clinic, given that they are not exposed to social pressure and the environment is created to accommodate reduced mobility (e.g., the deployment of adjustable chairs). On the other hand, altered behavior in the clinic could be due to over attention to one’s condition e.g., distress and fear in relation to therapy outcomes. Unfortunately, self-reports (e.g., diaries) often used by physiotherapists to assess people outside the clinics has been shown not to be reliable [29]. This is mainly because people are not often aware of how they move and what triggers increased pain or anxiety as the triggers may occur long before the perceived condition [62]. A ubiquitous system, capable of recognizing the activity context and continuously detecting protective behavior, can provide clinicians with a better understanding of the type of activity a person struggles with, or where the improvement is happening. As progress is not steady across all activities, clinicians together with the patient could work across the AoIs that need more attention. If connected to GPS and time, the system could further help contextualize the situation e.g., to understand other factors that may add pressure to the activity like climbing stairs under social pressure during busy hours. Beyond a summarization of frequency and well-designed visualizations, the system output can be contextualized into the environment as well. In a study [62], the authors show how a photo diary of the places or situation people struggle with lead to a more

effective patient-clinician interaction. Our ubiquitous HAR-PBD system could e.g., be integrated into such photo diary to catch attention or suggest recording the environment where protective behavior is recurrent in a particular AoI. Further, the system can be improved to detect which phases of an activity are more difficult and develop interventions to improve such phases (e.g., to start by sitting on a higher chair and progressively switch to a lower one, and remind to move the feet backward before standing up rather than relying solely on arm support and unhelpful muscle tensions).

Patient-oriented Ubiquitous Self-management. Patients find it very difficult to implement movement strategies learnt in the clinic to their everyday life. This is due to the complexity of the real word (e.g., the environment, social demand, variety of activities and responsibility etc) and also to their poor proprioceptive system as well as the emotional states [37]. In [29, 79], the authors show how a ubiquitous system that transforms real-time movements (of specific body parts) into sound (sonification) could increase awareness in people with chronic pain of their body capabilities and facilitate the application of movement strategies from clinic to self-managements. The study also shows the importance of providing such intervention when the person needs it rather than at all time. Instead of providing continuous feedback and advices, our HAR-PBD architecture can help decide when advices are needed to avoid being patronizing or a nuisance. Based on the frequency of protective behavior during specific activities, the system could identify if some support or advices are necessary. Beyond bodily awareness intervention, reminders of breathing and breaks can be suggested when protective behavior is detected over longer periods of time (e.g., more than 5 minutes). Taking breaks and relaxation are critical pacing strategies to avoid tension that could lead to setbacks and prolonged days in bed. In addition, as in-door environments and objects are being integrated with sensors, the interaction of the user with them could be further leveraged to provide even more appropriate feedback to tailor activity and re-organize the home, which was reported by patients to be a beneficial function they would expect from such ubiquitous system [29]. Finally, during exercise, the system can provide dedicated suggestions or exercise plans based on the frequency of protective behavior detected.

Beyond Chronic-pain Management to Next-stage Human Activity Analysis. Beyond supporting the management of chronic pain, our proposed hierarchical architecture could have applications in a variety of context where the ubiquitous HAR technology is developed. For example, ubiquitous HAR technology is opening new platform to aid workers in the context of factory assembly lines [15], to support them in their workspace activities, e.g., to identify and help correct mistakes, aid training and establish human-robot collaboration. Meanwhile, another interesting application is to help workers from the wellbeing perspective, such as to reduce mental or physical stress. Our architecture can be integrated into the system to leverage the HAR to detect cue of fatigue or pain avoidance. Such system could help identify the need of a break, adjust better timetabling of working shifts, thus, to avoid developing musculoskeletal condition, a notable issue in the manufactory industry nowadays. In this context, the number of sensors could be reduced to fit the specific needs of the types of activity and the type of movement behavior that would be exhibited therein. For instance, workers washing cars would generally do reach-forward and bend-down movement for a long period of time; workers in airplane manufacturing plants could be assigned to drilling thousands of screws in the wing of an airplane that requires keeping their back or neck bent backward under the wing for a long time while carrying heavy drillers; workers building furniture would be standing for long period of time or bend-down and reach-forward to chase the production as they are often paid by number of pieces produced [31]. Toward such need, given the evaluation conducted in Section 5.5, the basic component of GC-LSTM used in our architecture should be able to adapt to the input collected with different number of sensors attached to various places.

Another context of applications where ubiquitous computing is very active is to support people for healthcare purposes. For instance, the limb movement was assessed to screen perinatal stroke in infants [8], while the arm movement was adopted to track the everyday rehabilitation of stroke patients [75]. For these works, the integration of our hierarchical architecture can establish the link between the type of activity/movement performed and the behavior category (e.g., good or poor rehabilitation engagement for [75]). Such activity-aware functions could bring in more in-depth understanding of the user’s movement and open opportunities for personalized support.

6.3 Sensor network size: is being small always the best criteria?

A position often taken in the field of ubiquitous HAR is the use of minimalistic sets of sensors due to user acceptability. We challenge this view that equates increase in acceptability with decrease in number of sensors. This may be the case in situations where the benefit of using such sensors VS. the cost of wearing many sensors is possibly weak (e.g., detecting the number of push-up during a gym session) or in the situation where using even one sensor is already challenging (e.g., detecting if a person with dementia is eating). However, in the context of chronic pain, patients highlighted the wide benefits that support built of pain-related recognition system could bring to their ability to functioning (e.g., maintaining a job, contributing to family life, enjoy outing with friends, etc.) [29] [62], and possibly to improvement in their overall wellbeing (e.g., less use of medicines and reduced incident of depression). We would argue that such individual and critical benefits would counter the issues related to wearing a larger number of sensors, if such number would increase the feasibility of providing the right support. We should also consider that sensors are becoming increasingly cheaper, more accurate and wearable (e.g., invisible, washable or transferable between clothes [76]), making the burden or embarrassment of wearing a larger set of sensors to slowly disappear. In [65], patients stated their openness to wear sensors if these could be discrete, washable or interchangeable between clothes. It should also be noted that such wearable device may not be necessary at all the time even if these are long-term conditions. Previous studies on such feedback devices have shown that such technology may be used intermittently according to the fluctuating needs created by the chronic condition (e.g., ‘good days’ VS. ‘bad days’, training phases of self-management) [29] [36] [79]. Finally, given the reduction in cost that improvement in self-management would bring to the state and the national health system, we can expect an increase attention to the wearability of such sensors by the industry and related research communities, which is already happening in the context of stroke patients as wearable garments are created to detect the need of support [75]. We hence argue that ubiquitous wearable does not means a small set of sensors but a set of sensors whose use is sufficiently effective and beneficial in comparison to the cost. Hence, research with a larger set of sensors is needed to understand what is feasible and then work can be carried out to understand how to improve. In Section 5.5, a competitive PBD performance is seen by only using 14 joints of one side of the body. This informs the possibility of using a smaller sensor set to achieve comparable PBD performance, as well as shows the benefit of using body configuration knowledge e.g., the movement of one side of the body may provide similar information for PBD. We can build on such exploration in the use of fewer IMUs to investigate how the sensor set could be configured to address the need of specific individuals.

7 Conclusion

Ubiquitous technologies open new opportunities to support people with chronic pain during their everyday self-management. In this paper, we targeted PBD in continuous movement data as the critical first step. We proposed a hierarchical HAR-PBD architecture to recognize the varying context of activity to aid the detection of protective behavior simultaneously. An adapted CFCC loss was also used to alleviate the data imbalances during training. Our evaluation with data from real patients suggested that the activity type information is effective to aid PBD in continuous data, leading to a notable improvement over the baseline (macro F1 score of 0.73 and PR-AUC of 0.52 VS. macro F1 score of 0.66 and PR-AUC of 0.44), and is more impactful than just solving the data imbalances (macro F1 score of 0.71 and PR-AUC of 0.48). The best result was achieved by combining the hierarchical architecture with CFCC loss, with macro F1 score of 0.81 and PR-AUC of 0.60. Additionally, in Section 5.1, we verified that graph representation is indeed improving the PBD performance. In Section 5.4, we showed that it is feasible to jointly train the hierarchical HAR-PBD architecture. However, future work needs to find a better approach to gain mutual improvement between the HAR and PBD modules. In Section 5.5, we justified the importance of full-body movement data comprising 22 joints (macro F1 score of 0.66) to continuous PBD, but showed also the possibility of using fewer joints (macro F1 score of 0.57, 0.62, and 0.55 with 15-, 14- and 7-joint data respectively). To enable a compact sensor network, a better graph structure could be designed rather than merely constructing the human body. In the subsequent research, we hope to build on the findings of this paper to establish a ubiquitous system, considering real-world scenarios and designing proper interactions between the user and system.

REFERENCES

- [1] Vakanski, A et al. "Mathematical modeling and evaluation of human motions in physical therapy using mixture density neural networks." *Journal of physiotherapy & physical rehabilitation* 1.4 (2016).
- [2] de Gelder, B. "Why bodies? Twelve reasons for including bodily expressions in affective neuroscience". *Philosophical Transactions of the Royal Society B: Biological Sciences*, 364(1535), 3475–3484, (2009).
- [3] Kleinsmith, Andrea et al. "Affective body expression perception and recognition: A survey." *IEEE Transactions on Affective Computing* 4.1 (2013): 15-33.
- [4] Olugbade, Temitayo A., et al. "Automatic Detection of Reflective Thinking in Mathematical Problem Solving based on Unconstrained Bodily Exploration." *arXiv preprint arXiv:1812.07941* (2018).
- [5] Singh, A., et al. "Motivating People with Chronic Pain to do Physical Activity: Opportunities for Technology Design." In *International Conference on Human Factors in Computing Systems (CHI)* (pp. 2803–2812, (2014).
- [6] Joshi, Jyoti, et al. "Can body expressions contribute to automatic depression analysis?" *IEEE International Conference and Workshops on Automatic Face and Gesture Recognition (FG)*, IEEE, (2013).
- [7] Akther, Sayma, et al. "mORAL: An mHealth Model for Inferring Oral Hygiene Behaviors in-the-wild Using Wrist-worn Inertial Sensors." *Proceedings of the ACM on Interactive, Mobile, Wearable and Ubiquitous Technologies (IMWUT)* 3.1 (2019).
- [8] Gao, Yan, et al. "Towards Reliable, Automated General Movement Assessment for Perinatal Stroke Screening in Infants Using Wearable Accelerometers." *Proceedings of the ACM on Interactive, Mobile, Wearable and Ubiquitous Technologies (IMWUT)* 3, no. 1 (2019).
- [9] Hammerla, Nils Y. et al. "Deep, convolutional, and recurrent models for human activity recognition using wearables." *arXiv preprint arXiv:1604.08880*, (2016).
- [10] Guan, Yu et al. "Ensembles of deep lstm learners for activity recognition using wearables." *Proceedings of the ACM on Interactive, Mobile, Wearable and Ubiquitous Technologies (IMWUT)* 1.2, (2017): 11.
- [11] Morales, Francisco Javier Ordóñez et al. "Deep convolutional feature transfer across mobile activity recognition domains, sensor modalities and locations." *Proceedings of the 2016 ACM International Symposium on Wearable Computers (ISWC)*. ACM, (2016).
- [12] Zeng, Ming, et al. "Understanding and improving recurrent networks for human activity recognition by continuous attention." In *Proceedings of the 2018 ACM International Symposium on Wearable Computers (ISWC)*, pp. 56-63. ACM, (2018).
- [13] Murahari, Vishvak S. et al. "On attention models for human activity recognition." In *Proceedings of the 2018 ACM International Symposium on Wearable Computers (ISWC)*, pp. 100-103. ACM, (2018).
- [14] Du, Xin et al. "Transfer learning across human activities using a cascade neural network architecture." In *Proceedings of the 23rd International Symposium on Wearable Computers (ISWC)*, pp. 35-44. ACM, (2019).
- [15] Qingxin, Xia, et al. "Unsupervised Factory Activity Recognition with Wearable Sensors Using Process Instruction Information." *Proceedings of the ACM on Interactive, Mobile, Wearable and Ubiquitous Technologies (IMWUT)* 3, no. 2 (2019): 60.
- [16] Adaimi, Rebecca et al. "Leveraging Active Learning and Conditional Mutual Information to Minimize Data Annotation in Human Activity Recognition." *Proceedings of the ACM on Interactive, Mobile, Wearable and Ubiquitous Technologies (IMWUT)* 3, no. 3 (2019).
- [17] Yan, Sijie, et al. "Spatial temporal graph convolutional networks for skeleton-based action recognition." In *Thirty-Second AAAI Conference on Artificial Intelligence (AAAI)*. (2018).
- [18] Si, Chenyang, et al. "Skeleton-based action recognition with spatial reasoning and temporal stack learning." *Proceedings of the European Conference on Computer Vision (ECCV)*, pp. 103-118. (2018).
- [19] Shahroudy Amir et al. "Ntu rgb+ d: A large scale dataset for 3d human activity analysis." *IEEE conference on computer vision and pattern recognition (ICCV)*, pp. 1010-1019. (2016).
- [20] Kay, Will et al. "The kinetics human action video dataset." *arXiv preprint arXiv:1705.06950* (2017).
- [21] Stiefmeier, Thomas, et al. "Wearable activity tracking in car manufacturing." *IEEE Pervasive Computing* 2 (2008): 42-50.
- [22] Roggen, Daniel, et al. "Collecting complex activity datasets in highly rich networked sensor environments." *Networked Sensing Systems (INSS), Seventh International Conference on*. IEEE, (2010).

- [23] Reiss, Attila et al. "Introducing a new benchmarked dataset for activity monitoring." International Symposium on Wearable Computers (ISWC), IEEE, (2012).
- [24] Si, Chenyang et al. "An Attention Enhanced Graph Convolutional LSTM Network for Skeleton-Based Action Recognition." In Proceedings of the IEEE Conference on Computer Vision and Pattern Recognition (CVPR), pp. 1227-1236. (2019).
- [25] San-Segundo, Rubén et al. "Segmenting human activities based on HMMs using smartphone inertial sensors." Pervasive and Mobile Computing 30 (2016): 84-96.
- [26] Krishnan, Narayanan C et al. "Activity recognition on streaming sensor data." Pervasive and mobile computing 10 (2014): 138-154.
- [27] Yala, Nawel et al. "Feature extraction for human activity recognition on streaming data." International Symposium on Innovations in Intelligent Systems and Applications (INISTA), pp. 1-6. IEEE, (2015).
- [28] Yao, Ting et al. "Exploring visual relationship for image captioning." In Proceedings of the European conference on computer vision (ECCV), pp. 684-699. (2018).
- [29] Singh, A. et al. "Supporting Everyday Function in Chronic Pain Using Wearable Technology." Proceedings of the 2017 CHI Conference on Human Factors in Computing Systems, 3903–3915, (2017).
- [30] Takuya Akiba et al. "Optuna: A Next-generation Hyperparameter Optimization Framework." In KDD, (2019).
- [31] Michalos, George et al. "Workplace analysis and design using virtual reality techniques." CIRP Annals 67, no. 1 (2018): 141-144.
- [32] Aung, M. S. H et al. "The automatic detection of chronic pain- related expression: requirements, challenges and a multimodal dataset." IEEE Transactions on Affective Computing, 7(4), 1–18, (2016).
- [33] Keefe, F. J. et al. "Development of an observation method for assessing pain behavior in chronic low back pain patients." Behavior Therapy, (1982).
- [34] Vlaeyen, J. W. S. et al. "Fear-avoidance and its consequences in chronic musculoskeletal pain: A state of the art." Pain, 85 (3), 317-332, (2000).
- [35] Asghari, A et al. "Pain self-efficacy beliefs and pain behaviour: A prospective study." Pain, 94 (1), 85-100, (2017).
- [36] Olugbade, T. A. et al. "Human Observer and Automatic Assessment of Movement Related Self-Efficacy in Chronic Pain: from Movement to Functional Activity." IEEE Transaction on Affective Computing. (2018).
- [37] Olugbade, T. A et al. "How Can Affect Be Detected and Represented in Technological Support for Physical Rehabilitation?" ACM Transactions on Computer-Human Interaction, 26 (1), 1, (2019).
- [38] Wang, J. et al. "Mining actionlet ensemble for action recognition with depth cameras." Proceedings of the IEEE Conference on Computer Vision and Pattern Recognition (CVPR). (2012).
- [39] Fernando, B et al. "Modeling video evolution for action recognition." Proceedings of the IEEE Conference on Computer Vision and Pattern Recognition (CVPR), 5378–5387, (2015).
- [40] Chongyang Wang et al. "Recurrent network based automatic detection of chronic pain protective behavior using MoCap and sEMG data." Proceedings of the 23rd International Symposium on Wearable Computers (ISWC), pp. 225-230. ACM, (2019).
- [41] Lee, Inwoong, et al. "Ensemble deep learning for skeleton-based action recognition using temporal sliding LSTM networks." IEEE International Conference on Computer Vision (ICCV). IEEE, (2017).
- [42] Zhang, Songyang et al. "On geometric features for skeleton-based action recognition using multilayer lstm networks." Applications of Computer Vision (WACV), IEEE Winter Conference on. IEEE, (2017).
- [43] Ke, QiuHong et al. "A new representation of skeleton sequences for 3d action recognition." In Proceedings of the IEEE conference on computer vision and pattern recognition (CVPR), pp. 3288-3297. (2017).
- [44] Du, Y. et al. "Hierarchical recurrent neural network for skeleton based action recognition". Proceedings of the IEEE conference on computer vision and pattern recognition (CVPR), 1110–1118, (2015).
- [45] J. Liu et al. "Spatio-temporal lstm with trust gates for 3d human action recognition". Proceedings of the European Conference on Computer Vision (ECCV), (2016).
- [46] Liu, Jun et al. "Global context-aware attention lstm networks for 3d action recognition." Proceedings of the IEEE Conference on Computer Vision and Pattern Recognition (CVPR), pp. 1647-1656. (2017).

- [47] Li, Maosen et al. "Actional-Structural Graph Convolutional Networks for Skeleton-based Action Recognition." In Proceedings of the IEEE Conference on Computer Vision and Pattern Recognition (CVPR), pp. 3595-3603. (2019).
- [48] Shi, Lei et al. "Skeleton-Based Action Recognition with Directed Graph Neural Networks." In Proceedings of the IEEE Conference on Computer Vision and Pattern Recognition (CVPR), pp. 7912-7921. (2019).
- [49] Shi, Lei et al. "Two-Stream Adaptive Graph Convolutional Networks for Skeleton-Based Action Recognition." In Proceedings of the IEEE Conference on Computer Vision and Pattern Recognition (CVPR), pp. 12026-12035. (2019).
- [50] Gu, Chunhui et al. "Recognition using regions." IEEE Conference on Computer Vision and Pattern Recognition (CVPR), pp. 1030-1037, (2009).
- [51] B. Alexe et al. "Measuring the objectness of image windows." PAMI, (2012).
- [52] A. Humayun et al. "RIGOR: Reusing Inference in Graph Cuts for generating Object Regions." IEEE Conference on Computer Vision and Pattern Recognition (CVPR), (2014).
- [53] Pinheiro, Pedro O., et al. "Learning to refine object segments." In European Conference on Computer Vision (ECCV), pp. 75-91. Springer, Cham, (2016).
- [54] Duvenaud, David K et al. "Convolutional networks on graphs for learning molecular fingerprints." Advances in neural information processing systems (NIPS), pp. 2224-2232. (2015).
- [55] Niepert, Mathias et al. "Learning convolutional neural networks for graphs." International conference on machine learning (ICML), pp. 2014-2023. (2016).
- [56] A. Krizhevsky et al. "ImageNet classification with deep convolutional neural networks." Advances in neural information processing systems (NIPS), (2012).
- [57] Girshick, Ross et al. "Rich feature hierarchies for accurate object detection and semantic segmentation." In Proceedings of the IEEE conference on computer vision and pattern recognition (CVPR), pp. 580-587. (2014).
- [58] S. Ren et al. "Faster R-CNN: Towards real-time object detection with region proposal networks." Advances in neural information processing systems (NIPS), (2015).
- [59] Lin, Tsung-Yi et al. "Focal loss for dense object detection." Proceedings of the IEEE international conference on computer vision (ICCV), pp. 2980-2988. (2017).
- [60] Cui, Yin et al. "Class-balanced loss based on effective number of samples." Proceedings of the IEEE Conference on Computer Vision and Pattern Recognition (CVPR), pp. 9268-9277. (2019).
- [61] Hochreiter, Sepp et al. "Long short-term memory." Neural computation 9, no. 8 (1997): 1735-1780.
- [62] Felipe, Sergio et al. "Roles for personal informatics in chronic pain." 2015 9th International Conference on Pervasive Computing Technologies for Healthcare (PervasiveHealth), pp. 161-168, (2015).
- [63] Kipf, T. N. et al. "Semi-supervised classification with graph convolutional networks". Proceedings of International Conference on Learning Representations (ICLR), (2017).
- [64] Chongyang Wang et al. "Learning Bodily and Temporal Attention in Protective Movement Behavior Detection." Proceedings of IEEE International Conference on Affective Computing and Intelligent Interaction Demos and Workshops (ACIIW), (2019).
- [65] Swann-Sternberg et al. "User needs for technology supporting physical activity in chronic pain." In CHI'12 Extended Abstracts on Human Factors in Computing Systems, pp. 2441-2446. 2012.
- [66] LeCun, Yann et al. "Deep learning." Nature, 521, no. 7553 (2015): 436-444.
- [67] Kingma, Diederik P. et al. (2014). "Adam: A method for stochastic optimization." arXiv preprint arXiv:1412.6980.
- [68] Cook, K. et al. "Development and validation of a new self-report measure of pain behaviors." Pain, 154(12), 2867-2876, (2013).
- [69] Kleinsmith, Andrea et al. "Automatic recognition of non-acted affective postures." IEEE Transactions on Systems, Man, and Cybernetics, Part B (Cybernetics), 41, no. 4 (2011): 1027-1038.
- [70] N. Lawrence, "Matlab motion capture toolbox." <http://inverseprobability.com/mocap/>
- [71] Rivas, Jesús Joel, et al. "Automatic Recognition of Multiple Affective States in Virtual Rehabilitation by Exploiting the Dependency Relationships." In 2019 8th International Conference on Affective Computing and Intelligent Interaction (ACII), pp. 1-7. IEEE, (2019).
- [72] Van Asch, Vincent. "Macro-and micro-averaged evaluation measures." Belgium: CLiPS, 49 (2013).
- [73] Saito, Takaya et al. "The precision-recall plot is more informative than the ROC plot when evaluating binary classifiers on imbalanced datasets." PloS one, 10, no. 3, (2015).

- [74] Karg, Michelle et al. "Body movements for affective expression: A survey of automatic recognition and generation." *IEEE Transactions on Affective Computing* 4, no. 4 (2013): 341-359.
- [75] Halloran, Shane et al. "Remote monitoring of stroke patients' rehabilitation using wearable accelerometers." In *Proceedings of the 23rd International Symposium on Wearable Computers (ISWC)*, pp. 72-77. (2019).
- [76] Kang, Sung-Won et al. "The development of an IMU integrated clothes for postural monitoring using conductive yarn and interconnecting technology." *Sensors* 17, no. 11 (2017): 2560.
- [77] C. Johannes, T. et al. "The prevalence of chronic pain in United States adults." *J Pain*. 11 (11), pp. 1230-9, (2010).
- [78] Volta, Erica et al. "Analysis of cognitive states during bodily exploration of mathematical concepts in visually impaired children." In *2019 8th International Conference on Affective Computing and Intelligent Interaction (ACII)*, pp. 1-7. IEEE, (2019).
- [79] Singh, Aneesha et al. "Go-with-the-flow: tracking, analysis and sonification of movement and breathing to build confidence in activity despite chronic pain." *Human-Computer Interaction* 31, no. 3-4 (2016): 335-383.
- [80] Sullivan, M. J. L. et al. "The influence of communication goals and physical demands on different dimensions of pain behavior." *Pain*, 125(3), 270–277, (2006).
- [81] C. Drummond, R. C. Holte, et al. "Class imbalance, and cost sensitivity: why under-sampling beats over-sampling." In *ICML Workshop*, (2003).
- [82] C. Huang et al. "Learning deep representation for imbalanced classification." In *CVPR*, (2016), 1, 2.